Opportunities for Increased Efficiency in Monochromatic Photovoltaic Light Conversion

Daixi Xia*, Matthew M. Wilkins*†, Sanmeet S. Chahal*, Christopher E. Valdivia†, Karin Hinzer†*, and Jacob J. Krich*†

*Department of Physics, University of Ottawa, Ottawa, ON, K1N 6N5, Canada

†School of Electrical Engineering and Computer Science, University of Ottawa, Ottawa, Ontario, K1N 6N5, Canada

***Abstract* — We study efficiency loss mechanisms and the potential for improvement of a record-setting monochromatic photovoltaic device, which has demonstrated efficiency of 70% at 830 nm. We combine experimental and modeling-based estimates of losses due to reflection, transmission, thermalization, and series resistance into an extended detailed-balance model that further includes losses due to nonradiative recombination, quantified by an external radiative efficiency (ERE). From the device's efficiency, we estimate ERE $\geq$ 10%. The device efficiency could be improved by increased material quality, operation at a longer wavelength closer to the GaAs band gap, and increased light intensity. Each order of magnitude increase in incident light intensity or material ERE increases the efficiency by 4% absolute. Redesigning the device to operate at 850 nm reduces thermalization losses by 2% absolute. Overall device efficiency over 80% could be attained by combining these opportunities.**

***Index Terms* — photovoltaic cells, semiconductor devices, energy conversion, semiconductor device modeling**

I. Introduction

A monochromatic photovoltaic light converter – a phototransducer – converts narrow-band photonic energy into electricity. A high efficiency phototransducer enables several applications, including powering electronics through optical fiber. Inherently, an optical power transfer system is electrically isolated and protected from electromagnetic disturbances in the surroundings. As well, an optical source in the near infrared has small losses over long distance (4.5% over 100 m at 830 nm) in a silica fiber [1]. Hence, monochromatic photovoltaics are useful for many systems of telecommunication, biomedical engineering, electric vehicles and utilities, which sometimes require circuits immune to electromagnetic noise.

The detailed balance limit for monochromatic photovoltaic light conversion efficiency was shown by Green to be 100%, with the highest efficiencies requiring high input light intensity [2]. In previous architectures, an experimental monochromatic phototransducer showed conversion efficiency up to 58% with single junction cells in a series-connected architecture [3].

In 2016, our collaborators demonstrated a breakthrough in phototransducer efficiency with a 70% light-to-electricity conversion efficiency in a vertically-stacked multi-junction GaAs system [4]. In order to determine the best path forward to improve on this efficiency, we conduct a detailed study of the loss mechanisms of the record-setting device and incorporate them into a detailed-balance model of an equivalent single-junction device. We extend Green's detailed balance theory to include non-unity external radiative efficiency (ERE), allowing the detailed balance model to include non-radiative recombination.

II. Losses in Record-Setting Device

We introduce the 70% efficient phototransducer and describe its known sources of inefficiency due to thermalization, reflection, transmission, and series resistance. It is comprised of five GaAs p-n junctions separated by tunnel junctions, as illustrated in Figure 1 [4]. The phototransducer has a p-doped GaAs substrate, with a full coverage bottom contact. Each junction includes (from bottom to top) GaInP back surface

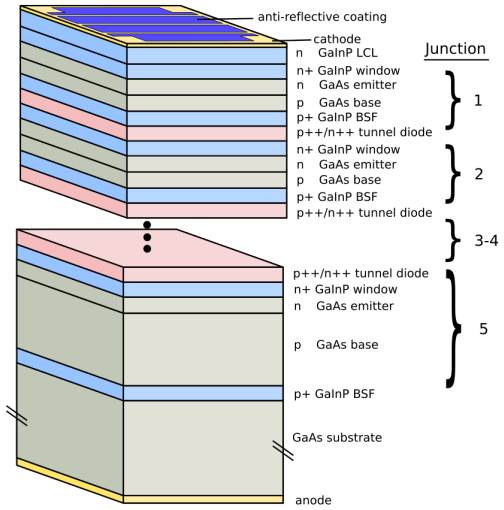

Fig. 1. Layer structure of a monochromatic phototransducer with five series-connected GaAs p-n junctions. Each junction is capped with a window layer at the front and a back surface field (BSF) layer at the back. A thick lateral conduction layer (LCL) enables current to spread to the gridlines.

field, p-doped GaAs base, thin n-doped GaAs emitter and n^+ GaInP front surface field (window). The lateral conduction layer of the top segment is designed to be extra-thick in order to allow carriers to reach the top contact with little loss. The top of the device has a gridline patterned contact. The voltage output of a single-junction cell is limited by the material's band gap, while a multi-junction design allows high voltage output from a single cell, eliminating fabrication complexities of a multi-cell array.

The segment thicknesses must be chosen to ensure current-matching at the operating wavelength, and the device is designed for an 830 nm (1.49 eV) input light source, which operated at 8 W/cm^2 with a FWHM of $\delta\epsilon = 1.8$ meV (i.e., FWHM of 1 nm). The GaAs band gap is at 870.7 nm (1.424 eV), so the device immediately loses 4% efficiency due to thermalization of the carriers to the GaAs band edge. This effect is included in the detailed balance model (see Section III).

We measure the reflectance loss at 830 nm to be 2%. Light transmitted to the substrate is considered lost and is estimated to be approximately 1% of the input light using a transfer matrix method calculation of the device transmission [5]. We include these losses due to transmission and reflectance in the detailed balance calculation of Section III as a reduced absorbance.

Resistive losses, on the other hand, are not directly included in the detailed balance model. We have made a detailed SPICE model of the 5-junction device and estimate the resistive loss due to conduction in the semiconductor to be 1% [6]–[8]. Resistive losses in the grid fingers, the metalized coating on the busbars or back contacts are estimated to be similar, for total resistance losses of 2%. We therefore estimate that an equivalent device without series resistance would be over 72% efficient. We call this estimate the *internal efficiency*, which we can compare to detailed balance calculations. This internal efficiency allows us to determine a lower limit on the external radiative efficiency of the device and thus to determine the prospects for increasing efficiency by improving material quality.

III. Detailed Balance Model

A. Detailed Balance Condition

The detailed balance formalism allows determination of the thermodynamic limiting efficiency of photovoltaic devices. If each photon absorbed produces one excited electron-hole pair, then in steady-state operation, the collected current from a device must equal the difference between the number of photons it absorbs and the number of excited electrons that recombine [9]. If the device has infinite carrier mobility, then the electron and hole quasi-Fermi levels are uniform through the device and the radiative recombination can be expressed in terms of the applied voltage [10]. We begin with the simplest case where all recombination is radiative, in which the current J can be expressed in terms of the applied voltage V as

$$J/q = \int_0^\infty a(E) n_s(E) \mathrm{d}E - \frac{2\Delta\Omega}{h^3 c^2} \int_0^\infty \frac{a(E) E^2}{e^{(E-qV)/kT} - 1} \mathrm{d}E \quad (1)$$

where the first term is the absorbed photon flux and the second term is the emitted photon flux, with $a(E)$ the photon-energy-dependent absorbance, $n_s(E)$ the input photon flux density, which in the case of a phototransducer has a small bandwidth, q the electric charge, h Planck's constant, c the speed of light, T the temperature, k Boltzmann's constant, and $\Delta\Omega$ the solid angle into which photons are emitted.

The experimental device has a multi-junction architecture, while our detailed balance model is for an analogous single-junction device. Our extended detailed-balance model captures the physics of incomplete absorption, thermalization, and radiative and nonradiative recombination (see Sec. III-C), but predicts a high-current low-voltage output, where the experimental device has a low-current high-voltage output. We believe that the fundamental limiting efficiencies of the multi-junction device are well captured by the single-junction detailed balance model, but development of a multi-junction detailed balance model is required for confirmation.

B. Absorbance and Input Spectrum

Transparency and thermalization losses can be understood with models for $a(E)$ and $n_s(E)$. We extend Green's formalism to incorporate such loss mechanisms into the detailed balance model. We consider $n_s(E)$ to be Gaussian with

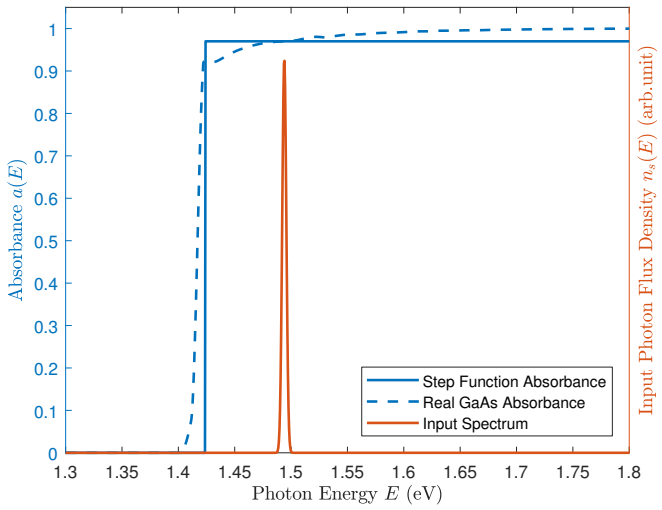

Fig. 2. Two models of device absorbance (blue lines, left axis). The solid line shows the step function absorbance, and the dashed line shows Beer-Lambert absorbance calculated from experimentally measured GaAs absorption coefficient [11]. The device thickness is chosen so that at the design wavelength of 830 nm, the absorbance is 97%. Right axis: Gaussian input photon flux density $n_s(E)$ for the considered device. The central frequency is detuned by $\delta E = 0.07$ eV from the band gap. The FWHM $\delta\epsilon = 1.8$ meV.

central photon energy E_s and FWHM $\delta\epsilon$. The central energy can be represented in terms of the detuning from the band gap: $\delta E = E_\mathrm{s} - E_\mathrm{g}$. We consider two models for $a(E)$, as illustrated in Figure 2: first, a step function equal to 0 for $E \leq E_g$ and a_0 for $E \geq E_g$; second, a Beer-Lambert absorption model with experimentally measured GaAs absorptivity with thickness chosen so $a(E) = a_0$ at 830 nm [11]. In the step-function model, $a(E) = a_0\Theta(E-E_\mathrm{g})$, where $a_0 = 0.97$ and Θ is the unit step function. With the step function absorbance model, Eq. (1) can be simplified to

$$J/q = \frac{1}{2}a_0\dot{N}\left[1-\mathrm{erf}\left(2\sqrt{\ln 2}\frac{\delta E}{\delta\epsilon}\right)\right] - \frac{2a_0\Delta\Omega}{h^3c^2}\int_{E_\mathrm{g}}^{\infty}\frac{E^2}{e^{(E-qV)/kT}-1}dE \quad (2)$$

where $\dot{N}$ is the total (energy integrated) input photon flux and erf is the standard error function.

Incident power is $P_{in} = \dot{N}(E_g + \delta E)$ and output power is $P_{out} = J(V)V$ which must be optimized over V. The maximum efficiency is $\eta = \frac{P_{out}}{P_{in}}$ at the optimum V. To illustrate the dependence of thermalization and transparency on δE and $\delta\epsilon$, Figure 3 shows optimum efficiency as a function of δE for different input linewidths $\delta\epsilon$. When the input radiation has a significant bandwidth $\delta\epsilon$, the optimal choice of detuning δE balances between the thermalization losses, which increase with δE, and transparency losses, which increase as δE becomes smaller than $\delta\epsilon$. For each $\delta\epsilon$, the maximum efficiency occurs when the transparency loss and thermalization loss are approximately equal, which requires $\delta E \approx \delta\epsilon$. This behavior is demonstrated in Figure 3 where narrower inputs give rise to higher maximum efficiencies at smaller detuning. As $\delta\epsilon \to 0$, the thermalization and transparency losses can be reduced to zero by choosing $\delta E \to 0$. In this fully monochromatic limit, the system would reach its highest efficiency. In contrast, the real absorbance model is less susceptible to transparency loss as $\delta E \to 0$, since the absorbance does not decrease to zero so abruptly (dashed lines).

C. Non-Radiative Recombination

We extend the results of [2] to include nonradiative processes by means of the external radiative efficiency, ERE. In the detailed-balance formalism, radiative recombination is a loss mechanism only if the photons exit the device and thus cannot be reabsorbed, whereas nonradiative recombination is always a loss mechansim. The ERE is the fraction of all losses (including both nonradiative recombination and photon emission) that are due to photon emission from the device. The ERE of a cell is experimentally measurable and is associated with both material quality and device architecture [12]. Still in the step-function absorbance model, the current density is modified from Eq. (2) with the inclusion of ERE

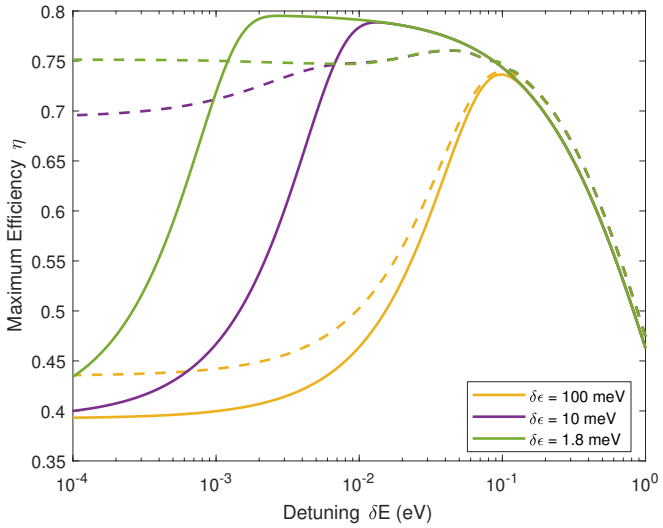

Fig. 3. Detailed balance efficiency as a function of input light detuning δE for different input linewidths $\delta\epsilon$, $\Delta\Omega = \pi$ and laser power density 8 W/cm^2. The solid lines are for the step function absorbance model and the dashed lines are for the real absorbance model. The experimental device has $\delta\epsilon = 1.8$ meV and $\delta E = 0.07$ eV. Note that in the real absorbance model, device thickness is set to absorb 97% of the photons at 830 nm, so transmission loss increases as δE is reduced. The peak efficiency of 76% could be improved by increasing device thickness.

as

$$J/q = \frac{1}{2}a_0\dot{N}\left[1-\mathrm{erf}\left(2\sqrt{\ln 2}\frac{\delta E}{\delta\epsilon}\right)\right] - \frac{2\pi a_0}{h^3c^2}\frac{\Delta\Omega}{ERE}\int_{E_\mathrm{g}}^{\infty}\frac{E^2}{e^{(E-qV)/kT}-1}dE \quad (3)$$

D. Normalized Intensity

Including the ERE does not significantly change the derivation of Green, nor does the presence of detuning δE. In the step-function absorbance case, the resulting efficiency depends on E_g/kT, δE, and the normalized input light intensity i,

$$i = \frac{h^3c^2}{2}\frac{\dot{N}\cdot ERE}{\Delta\Omega E_\mathrm{g}^2 kT}\frac{1}{2}\left[1-\mathrm{erf}\left(2\sqrt{\ln 2}\frac{\delta E}{\delta\epsilon}\right)\right]. \quad (4)$$

Then the (voltage dependent) efficiency can be written as

$$\eta = ma_0\left[1-\frac{1}{i}\ln\left(\frac{y+1}{y}\right)f\right]\left[1-\frac{kT}{E_\mathrm{g}}\ln(y+1)\right], \quad (5)$$

where $y = \exp[(E_\mathrm{g}-qV)/kT]-1$, $m = \frac{1}{2}\frac{1-\mathrm{erf}\left(2\sqrt{\ln 2}\frac{\delta E}{\delta\epsilon}\right)}{1+\frac{\delta E}{E_\mathrm{g}}}$ and f is a number close to 1, $1 \leq f \leq \left[1+2\frac{kT}{E_\mathrm{g}}+2\left(\frac{kT}{E_\mathrm{g}}\right)^2\right]$.

The experiment, with emission angle $\Delta\Omega = \pi$, $\delta E = 70$ meV, $\delta\epsilon = 1.8$ meV and laser intensity of 8 W/cm^2 [4], corresponds to a normalized intensity of $i = 0.0065 \cdot ERE$.

Device efficiency increases with i until saturating near unity, as shown in Figure 4. This normalized intensity shows that the same improvement in efficiency can be achieved by increasing the input photon flux, increasing the material quality (i.e., ERE), or restricting $\Delta\Omega$. The upper axis shows

how this normalized intensity corresponds to laser intensities, assuming that $\Delta\Omega = \pi$ and that δE and $\delta\epsilon$ are fixed to their values from the considered device. At the experimental intensity, with no nonradiative processes, the detailed balance calculation would predict $\eta = 76\%$, which is higher than the estimated internal efficiency of 72%, indicating that the ERE of the device is in fact less than 1, as expected. The normalized intensity corresponding to 72% efficiency is $i = 0.0006$. The device is thus estimated to have an ERE of 10%.

Even with realistic absorption profiles, where Eq. 5 does not strictly apply, i gives a very good estimate of a device's efficiency. In Figure 4, the detailed balance efficiency is also calculated based on the real GaAs absorbance model with varying intensities, using a_0, δE, $\delta\epsilon$ and ERE as for the step-function model. Both curves show the same increase of efficiency with i and nearly the same absolute efficiency. The step-function absorbance model overestimates the efficiency by about 1%, due to an underestimate of sub-bandgap photon emission. Due to this sub-bandgap absorbance, we do not extend the real absorbance model to input intensity higher than 10^4 W/cm^2. High intensity results in an operating voltage very close to the band gap, where in the real absorbance model, the absorbance is non-zero. Such lasing behavior is not captured in the current formalism. A generalized cell analysis including such effects is possible [13], and we expect it to give results similar to our step-function analysis with an asymptote at a slightly lower maximum η. Nevertheless, in the moderate-intensity regime, the step function model and i provide accurate and intuitive information on the relative efficiency improvements possible with changes to the physical parameters.

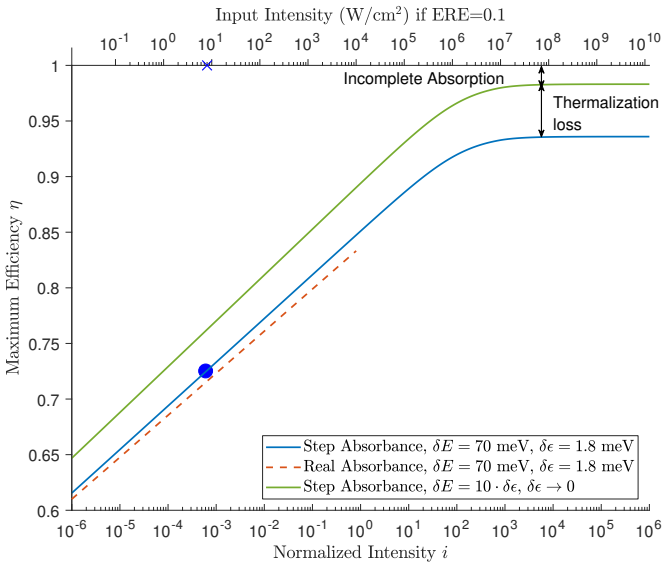

Fig. 4. Efficiency as a function of normalized intensity i (bottom axis), first calculated using the definition in Eq. 4, for a material with $E_g = 1.424$ eV and step function $a(E)$ with $a_0 = 0.97$ with detuning $\delta E = 0.07$ meV (blue curve). The line asymptotes at 92% due to finite detuning and incomplete absorption. The point with $\eta = 0.72$ shows the estimate of the internal efficiency of the 70% efficient device when series resistance is removed. The green curve is the efficiency in the monochromatic limit, where $\delta E = 10\delta\epsilon$ and $\delta\epsilon \to 0$. The line asymptotes at 97% due to incomplete absorption. The top axis shows the input intensity with $\delta\epsilon = 1.8$ meV, detuning $\delta E = 0.07$ eV, emission angle $\Delta\Omega = \pi$ and ERE= 10%. The device operates at 8 W/cm^2 [4], which is marked on the top axis. Efficiency is also calculated based on the real GaAs absorbance model illustrated in Figure 2, with δE, $\delta\epsilon$, ERE and $\Delta\Omega$ as above.

IV. Implications for High Efficiency

There are two important parameters that determine the efficiency of a phototransducer - the detuning to linewidth ratio $\frac{\delta E}{\delta\epsilon}$ and the normalized intensity i. In this section, we discuss possible improvement of efficiency based on these two parameters.

The current device was not designed at its theoretical optimal δE, as shown in Figure 3. If the input wavelength can be adjusted without changing its bandwidth, the efficiency can be improved by 2% absolute by decreasing the detuning to 0.03 meV. However, at a smaller detuning, more material is needed in order to achieve the same 97% effective absorbance, due to smaller GaAs absorptivity. For a detuning of 0.03 eV, the device would be 20% thicker than the present one to achieve the same absorbance. It is also worth noting that an LED light source with $\delta\epsilon$ 1 to 2 orders of magnitude larger gives a smaller window of optimum detuning as well as lower optimal efficiency. Yet a device with the current thickness, $\delta\epsilon$ increased by 2 orders of magnitude and carefully tuned central wavelength could have an efficiency similar to the current record-setting device, without requiring a laser input.

Increasing normalized intensity i also significantly improves the efficiency. As shown in Figure 4, increasing i by an order of magnitude would improve the efficiency by approximately 4%. This increase can be achieved by increasing input power density to 100 W/cm^2, restricting the emission angle $\Delta\Omega$ using a lens, or improving material quality (ERE), with each having a similar effect. The ERE of 10% predicted here is already very high among III-V devices, with the highest measured ERE= 22.5% for thin film GaAs [12]. Since further increases in material quality are difficult, improved efficiency from increased input power density seems to be the easiest method.

In summary, with 2% improvement from smaller detuning and 4% from increasing input intensity, combined with improvements in series resistance, reflection, and transmission, a device efficiency of over 80% appears reachable at an operating wavelength of 850 nm.

References

[1] B. E. A. Saleh and M. C. Teich, *Fundamentals of photonics*, 2nd ed. Hoboken, N.J: Wiley Interscience, 2007.

[2] M. A. Green, "Limiting photovoltaic monochromatic light conversion efficiency," *Progress in Photovoltaics: Research and Applications*, vol. 9, no. 4, pp. 257–261, 2001.

[3] A. Fahrenbruch, L. Lopez-Otero, J. Werthern, and Ta-Chung Wu, "GaAs- and InAlGaAs-based concentrator-type cells for conversion of power transmitted by optical fibers," in *25th IEEE Photovoltaic Specialists Conference*. Washington, DC, USA: IEEE, 1996, pp. 117–120.

[4] S. Fafard, M. C. A. York, F. Proulx, C. E. Valdivia, M. M. Wilkins, R. Arès, V. Aimez, K. Hinzer, and D. P. Masson, "Ultrahigh efficiencies in vertical epitaxial heterostructure architectures," *Applied Physics Letters*, vol. 108, no. 7, p. 071101, 2016.

[5] M. Wilkins, C. E. Valdivia, A. M. Gabr, D. Masson, S. Fafard, and K. Hinzer, "Luminescent coupling in planar opto-electronic devices," *Journal of Applied Physics*, vol. 118, no. 14, p. 143102, Oct. 2015.

[6] P. Sharma, A. W. Walker, J. F. Wheeldon, K. Hinzer, and H. Schriemer, "Enhanced Efficiencies for High-Concentration, Multijunction PV Systems by Optimizing Grid Spacing under Nonuniform Illumination," *International Journal of Photoenergy*, vol. 2014, 2014, Art. ID 582083.

[7] C. E. Valdivia, M. M. Wilkins, S. S. Chahal, F. Proulx, P.-O. Provost, D. P. Masson, S. Fafard, and K. Hinzer, "Many-junction photovoltaic device performance under non-uniform high-concentration illumination," *AIP Conference Proceedings*, vol. 1881, p. 070005, Sep. 2017.

[8] S. Chahal, M. M. Wilkins, D. P. Masson, S. Fafard, C. E. Valdivia, and K. Hinzer, "20-junction photonic power converter performance under non-uniform illumination calculated by 3d distributed circuit model (Conference Presentation)," in *Physics, Simulation, and Photonic Engineering of Photovoltaic Devices VI*, vol. 10099. International Society for Optics and Photonics, Apr. 2017, p. 1009908.

[9] W. Shockley and H. J. Queisser, "Detailed Balance Limit of Efficiency of *pn* Junction Solar Cells," *Journal of Applied Physics*, vol. 32, no. 3, pp. 510–519, 1961.

[10] P. Wurfel, "The chemical potential of radiation," *Journal of Physics C: Solid State Physics*, vol. 15, no. 18, pp. 3967–3985, 1982.

[11] S. Adachi, *Optical constants of crystalline and amorphous semiconductors: numerical data and graphical information*. Boston: Kluwer Academic Publishers, 1999.

[12] M. A. Green, "Radiative efficiency of state-of-the-art photovoltaic cells: Radiative efficiency of photovoltaic cells," *Progress in Photovoltaics: Research and Applications*, vol. 20, no. 4, pp. 472–476, 2012.

[13] M. A. Green, *Third generation photovoltaics: advanced solar energy conversion*. Berlin: Springer, 2003.